Temperature Response of Aqueous Solutions of a Series of Pyrene End-Labeled Poly(*N*-isopropylacrylamide)s Probed by Turbidimetry, Light Scattering, and Fluorescence

Mike Fowler[a], Jean Duhamel*[a], Xing Ping Qiu[b], Evgenyia Korchagina[b], Françoise M. Winnik*[b]

a) Institute for Polymer Research, Waterloo Institute for Nanotechnology, Department of Chemistry, University of Waterloo, Waterloo, ON N2L 3G1, Canada

b) Faculty of Pharmacy and Department of Chemistry, Université de Montréal, CP 6128 Succursale Centre Ville, Montréal QC H3C 3J7, Canada

Correspondence to: Jean Duhamel (E-mail: *jduhamel@uwaterloo.ca*)

((Additional Supporting Information may be found in the online version of this article.))

ABSTRACT

Aqueous solutions of a series of monodisperse poly(*N*-isopropylacrylamide)s end-labeled with either one or two pyrenes (Py_n-PNIPAMs with n = 1 or 2) were studied by turbidimetry, light scattering, and fluorescence. For a given polymer concentration and heating rate, the cloud point (T_c) of the Py_n-PNIPAM solution determined using turbidimetry was found to increase with the number-average molecular weight (M_n) of the polymer. The steady-state fluorescence spectra and time-resolved fluorescence decays of the Py_n-PNIPAM aqueous solutions were analyzed and all parameters retrieved from these analyses were found to be affected as the solution temperature passed through T_c, the solutions cloud point, and T_m, the temperature where dehydration of PNIPAM occurred. The trends obtained by fluorescence to characterize the aqueous Py_n-PNIPAM solutions as a function of temperature were found to be consistent with the model proposed for telechelic PNIPAM by F. M. Winnik et al. in 2006.

KEYWORDS: pyrene fluorescence, dynamic light scattering, poly(*N*-isopropylacrylamide), thermoresponsive, aggregation

INTRODUCTION

Aqueous solutions of poly(*N*-isopropylacrylamide) (PNIPAM) have been the subject of major scientific interest for over 50 years[1] and have been studied using a variety of techniques including viscometry,[2-4] turbidimetry,[3,5-8] light scattering,[4,8,9] fluorescence,[6,9-14] and neutron scattering.[15-18] The origin of this interest resides in the fact that PNIPAM possesses a lower critical solution temperature (LCST), also known as its cloud point (T_c), which is typically reported as 32 °C and is relatively insensitive to polymer concentration so long as the concentration is above 1 g/L.[19-23] PNIPAM transitions from soluble coils to dehydrated globules at T_c and these globules then form larger aggregates called mesoglobules.[19,24-27] The transition at T_c, also referred to as the coil-to-globule transition (CGT), occurs over a narrow temperature range because the process of hydration/dehydration is cooperative[15,28] and results in chains that adopt a pearl necklace conformation in

solution.[18] The value of T_c for a given PNIPAM solution depends on a number of factors that include the nature and distribution along the chain of chemical groups that can be incorporated randomly or at the chain ends, the polymer molecular weight, and the polymer concentration[8] if the solution is in the dilute regime. The nature of the end-groups has a particularly significant effect on telechelic PNIPAM, where hydrophobic end-groups cause T_c to decrease with decreasing molecular weight[7] and hydrophilic end groups result in the opposite trend.[29]

Since PNIPAM turns water-insoluble above T_c, a number of studies have examined the interactions that exist between PNIPAM and either small molecule surfactants[3,30,31] or hydrophobically modified water-soluble polymers which are not PNIPAM.[2,6] They have shown that the presence of hydrophobic aggregates in solution affects the dehydration-induced aggregation of PNIPAM causing changes in T_c, while PNIPAM is also capable of disrupting hydrophobic aggregates when it undergoes its CGT.[2,32] These effects are due to the dehydration of PNIPAM that occurs above T_c and results in the formation of less hydrophilic microdomains capable of interacting with hydrophobic groups.

Since the bridging induced by hydrophobic associations between hydrophobically modified water-soluble polymers such as Hydrophobically modified Ethoxylated Urethanes (HEURs), Hydrophobically Modified Alkali Swellable Emulsion copolymers (HASEs), or Hydrophobically Modified HydroxyEthyl Cellulose (HMHEC) often conveys industrially relevant viscoelastic properties to their aqueous solutions,[33,34] the modification of water-soluble PNIPAMs by covalent attachment of lipophilic groups (referred to as *lip*) bore the promise that temperature could be used as an additional parameter to further control the viscoelastic properties of aqueous solutions of *lip*-PNIPAMs. This realization led to a sustained scientific interest in understanding the complex interactions of *lip*-PNIPAMs that take place in water intra- and intermolecularly between the hydrophobic pendants and the PNIPAM backbone as a function of solution temperature. However the shear complexity of the different physical phenomena (hydrophobic associations, PNIPAM dehydration, macromolecular aggregation) occurring simultaneously in the aqueous solution led to the design of simpler *lip*-PNIPAM constructs such as telechelic monodisperse lip_2-PNIPAMs where two same hydrophobes were covalently attached to the ends of a monodisperse PNIPAM and the effects of these end-groups on the association mechanism have been investigated.[9,10,15-18,35,36] In essence such model compounds are the thermoresponsive equivalent of monodisperse HEURs and they are the focus of the present study. lip_2-PNIPAMs have been studied by light scattering, neutron scattering, fluorescence, and other techniques[9,10,15-18] and the results of these investigations have led to the establishment of a model describing the behaviour of aqueous solutions of lip_2-PNIPAM as the temperature increases. The key points of this model originally proposed by F. M. Winnik et al.[9,15] have been depicted in Scheme 1 and are discussed hereafter.

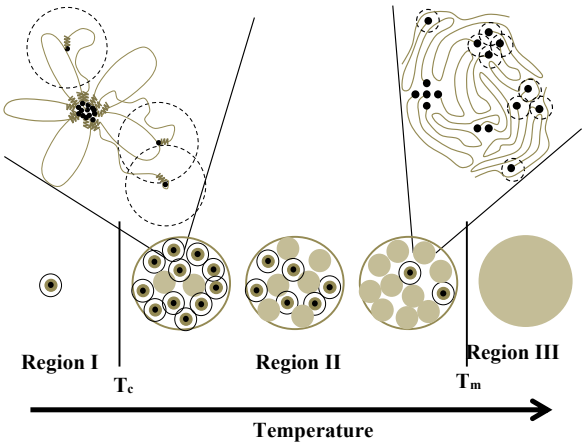

SCHEME 1 Effect of temperature on the distribution of the pyrene species and the morphology of the *lip*$_2$-PNIPAM chains. Color code: Black: pyrene; grey: dehydrated PNIPAM; white: solvated PNIPAM chains.

Below 20 °C, *lip*$_2$-PNIPAM forms stable flower-like micelles with a three layered onion-like structure. The innermost core is composed of the hydrophobes, the outermost shell is constituted of hydrated PNIPAM loops, and the middle region between the two consists of a mixture of water and dehydrated PNIPAM segments. As the temperature increases above 20 °C, the *lip*$_2$-PNIPAM solution enters the thermodynamic Regime I where segments of the PNIPAM loops in the shell begin to dehydrate and collapse into the middle region. Water is expelled from the middle region as the dehydrating chains of the shell collapse into it, leading to a constant volume for the middle region and a decrease in the volume of the shell.[17] As dehydrated PNIPAM chain segments also enter the hydrophobic core, the core becomes more hydrophilic.[9] This behaviour continues until T_c is reached, reported as 31 °C for the polymer used in these studies.

At T_c, the *lip*$_2$-PNIPAM solution enters Regime II where the micelles begin to associate with one another to form larger aggregates called mesoglobules. The apparent M_n of PNIPAM mesoglobules increases significantly while the internal fluidity of the mesoglobules decreases.[9,13] As the temperature approaches the stable mesoglobule temperature of 34 °C (T_m),[9] the mesoglobules increase in size while the hydrophobic cores of the micelles within the mesoglobules begin to dissolve and disperse throughout the mesoglobule. At the same time, additional water is expelled from the mesoglobules.[14] Above T_m, the *lip*$_2$-PNIPAM solution enters Regime III where mesoglobules stabilize and do not grow any further. At this stage, the mesoglobules are thought to have an "almost frozen nature".[15,17] In all three regimes, any structures formed, either micelles or mesoglobules, do not interact with one another if the polymer concentration is below 1 g/L.[15,17,18] While the solutions of *lip*$_2$-PNIPAM show an M_n-dependence for T_c, T_m is always found to equal 34 °C regardless of M_n.

This description of the dehydration of *lip*$_2$-PNIPAM with increasing temperature suggests that the hydrophobes experience some rather drastic changes in their environment, as *lip*$_2$-PNIPAM incorporated in rosette micelles at low temperature transitions from isolated micelles in aqueous solution where the hydrophobes are somewhat exposed to the water phase, to aggregated micelles inside a mesoglobule at T_c where the hydrophobes are much more protected from the aqueous phase, to the dehydration of PNIPAM in Regime II which induces the dispersion of the hydrophobes throughout the dehydrated PNIPAM matrix and a reduction in their mobility. As it turns out, the phenomena described above could be investigated by studying the fluorescence response of a series of *lip*$_2$-PNIPAMs where the two hydrophobic ends were replaced by two pyrene chromophores to yield Py$_2$-PNIPAM

constructs. Pyrene is ideally suited for such an investigation since it is hydrophobic and its fluorescence is sensitive to changes in its mobility and local concentration through pyrene excimer formation and its accessibility to the solvating medium through protective quenching.

To this end, a series of Py_n-PNIPAM samples (where *n* equals 1 or 2) were prepared with 1-pyrenebutyl groups to replace the octadecyl groups used in previous studies of *lip*$_2$-PNIPAM.[9,17,18,37] The behavior of the Py_n-PNIPAM samples was characterized not only by steady-state and time-resolved fluorescence, but also by turbidimetry and light scattering to establish the transition temperatures T_c and T_m. While turbidimetry and light scattering reported on the behaviour of the entire polymer chain, fluorescence provided information on the specific behaviour of the hydrophobes. The effect of temperature on the behavior of the pyrenyl groups was characterized as the temperature passed through T_c and T_m. The results obtained through this fluorescence study of the Py_n-PNIPAM samples established that the pyrenyl end groups responded to changes in solubility experienced by the macromolecule and the trends obtained from the fluorescence data appeared to fall within the framework provided by the model proposed by F.M. Winnik et al.[9,15,17]

EXPERIMENTAL

Materials. Water was deionized with a Milli-Q UF Plus system (Bedford, MA) such that it had a resistivity exceeding 18 MΩ·cm. The pyrene-labeled PNIPAM samples were prepared by reversible addition fragmentation chain transfer polymerization (RAFT) of NIPAM followed by end-group modification with a pyrenylbutyl derivative, as reported previously.[10] The degree of end-group substitution exceeded 75%. The number-average molecular weight (M_n) and polydispersity index of the samples are listed in Table 1. The following nomenclature was used to identify the samples: Py_1-PNIPAM refers to polymers singly-labeled with pyrene (or semi-telechelic), while Py_2-PNIPAM refers to the telechelic chains. The number in brackets denotes the M_n of the PNIPAM backbone in kg/mol. The unlabeled PNIPAM sample of 20 < Mw < 25 kg/mol (averaged to 22 kg/mol) was purchased from Sigma-Aldrich and used as received. Ethanol (HPLC grade reagent alcohol) was supplied by Fischer Scientific.

Solutions preparation. In order to avoid errors related to the hypochromicity of pyrenyl derivatives in water,[38] solutions of the polymers in ethanol were prepared first to determine the exact concentration of the Py_n-PNIPAM solutions, followed by solvent exchange from ethanol to water. Solutions of the polymers in ethanol were prepared, starting from dry polymer powder. The polymer concentrations were determined from the UV absorbance at 344 nm of the pyrenylbutyl substituent, using the molar extinction coefficient ε_{Py} = 42,250 $mol^{-1}.L.cm^{-1}$ of 1-pyrenebutanol in ethanol. Subsequently, aliquots of the solutions were transferred in separate vials, in amounts calculated to yield, upon dilution, aqueous solutions having an absorbance at 344 nm of 0.1 ([pyrene] = 2.4 µmol L^{-1}). The ethanol was removed under a stream of nitrogen. Desired amounts of water were added to the residues. The mixtures were vortexed briefly and kept at 4 °C for at least 30 minutes prior to measurements. This protocol yielded Py_n-PNIPAM solutions of identical pyrene concentration ([pyrene] = 2.4 µmol.L^{-1}) and polymer concentrations ranging from 9.5 mg.L^{-1} to 59.0 mg.L^{-1} (Table 1). The unlabeled PNIPAM

solution was prepared by dissolving a known weight of polymer in water to yield a 1 $g.L^{-1}$ stock solution and reducing the concentration via successive dilutions to the desired polymer concentration, namely 0.5 $g.L^{-1}$ for the turbidimetry measurements in Figure 1 or the concentration of the Py_n-PNIPAM solutions to determine the background scattering for subtraction from the fluorescence spectra (see Figure S3 and explanation in Data Analysis).

TABLE 1 Number-average molecular weight (M_n) and polydispersity index (PDI) of the PNIPAM samples and their concentrations for the fluorescence experiments.

Sample	M_n (kg/mol)	PDI	[Py_n-PNIPAM] (mg/L)
Py_2-PNIPAM(7K)	7.6	1.08	9.5
Py_2-PNIPAM(14K)	13.7	1.10	17
Py_2-PNIPAM(25K)	25.4	1.07	32
Py_2-PNIPAM(45K)	44.5	1.10	56
Py_1-PNIPAM(7K)	7.68	1.02	18
Py_1-PNIPAM(12K)	12.3	1.02	30
Py_1-PNIPAM(25K)	23.5	1.09	59
PNIPAM(22K)	20-25		

Instrumentation and methods. The phase transition temperature of Py_n-PNIPAM aqueous solutions was determined by turbidimetry measurements performed on a Varian Cary 100 Bio UV-Vis spectrophotometer equipped with a 6×6 multicell sample holder thermostatted with a Peltier controller and able to cover a temperature range between –10 and 100 °C. The absorbance at 500 nm was recorded as the temperature of aqueous Py_n-PNIPAM solutions (0.5 $g.L^{-1}$) was raised from 10 to 45 °C at a heating rate of 0.5 $°C.min^{-1}$ and absorbance readings were taken at every 0.25 °C.

Dynamic light scattering experiments were performed on an ALV GmbH instrument equipped with a CGS-3 goniometer and an ALV-5000 multiple digital time correlator. A He-Ne laser operating at a wavelength of λ_o = 632.8 nm was used as the light source. Before the measurements, all solvents and solutions were filtered through a 0.22 µm pore size filter. To confirm the transition temperatures obtained by turbidimetry, the phase transition temperature of aqueous Py_n-PNIPAM solutions (0.5 $g.L^{-1}$) was determined from the temperature-dependent scattering intensity measured at 90° of samples heated stepwise at an approximate rate of 0.5 $°C.min^{-1}$. Dynamic light scattering measurements were conducted with aqueous Py_n-PNIPAM solutions kept at 15 or 35 °C with polymer concentrations that were adjusted for the scattering intensity which was low at 15 °C and high at 35 °C where PNIPAM is soluble and insoluble, respectively. In addition, the phase transition temperature of dilute Py_n-PNIPAM solutions used for fluorescence measurements with polymer concentrations ranging between 10 and 60 $mg.L^{-1}$ was determined using the steady-state fluorometer. Solutions were irradiated at 500 nm in the fluorometer. The intensity of the scattered light from 490 to 510 nm was determined in 0.5 nm increments as a function of temperature for samples heated at a rate equivalent to 0.1 $°C.min^{-1}$ with 1 °C increments from 20 to 40 °C.

Steady-state fluorescence measurements were conducted using a Photon Technology International LS-100 steady-state fluorometer equipped with a continuous xenon lamp. Quartz fluorescence cells (VWR) with an inner cross section of 10 × 10 mm^2 were used and measurements were performed with a right angle geometry. They were placed in a

temperature-controlled cell holder thermostated by an external circulating water bath. Pyrene fluorescence spectra were acquired upon excitation at 342 nm. The excitation and emission slits were set at 2.0 and 1.0 nm, respectively. For each temperature setting, the spectra acquisition took about 1 minute. The temperature was increased in 1.0 °C increments. Samples were allowed to equilibrate for 10 min after each temperature change. Thus, the fluorescence experiments were conducted with an average heating rate of about 0.1 °C.min^{-1} and with aerated solutions.

The fluorescence decay profiles were obtained with a time-correlated single photon counter manufactured by IBH Ltd. using a NanoLED 340 nm diode as the excitation source. Samples were excited at 342 nm, and the emission wavelength was set at 375 nm and 510 nm for the pyrene monomer and excimer, respectively. The samples were placed in a 10 × 10 mm^2 fluorescence cell (VWR) and left to equilibrate at the set temperature for 10 minutes. Monomer and excimer decays acquisition took about 5 minutes before the temperature was raised by 1 °C to repeat the process. Thus the heating rate of the time-resolved fluorescence experiments can be estimated to equal 0.07 °C.min^{-1}. All decays were collected with the right angle geometry over 1,024 channels with a minimum of 20,000 counts taken at the decay maximum to ensure a high signal-to-noise ratio. A light scattering standard was used to determine the instrument response function (IRF).

Data analysis. The transmission-vs-temperature profile used to monitor the turbidity of the Py$_n$-PNIPAM aqueous solutions such as shown in Figures 1A or S1 in Supporting Information (SI) were analyzed as follows. The derivative of the transmittance with respect to temperature was determined, and T_c was taken as the point of intersection between the baseline and the rise in the derivative. An example of the determination of T_c by turbidimetry may be found in Figure S1.

A light scattering correction was applied to the analysis of the fluorescence spectra by subtracting the spectrum obtained from the light scattered by a non-fluorescently labeled PNIPAM(22K) solution at the same polymer concentration, scaled for intensity, from the fluorescence spectrum of the Py$_n$-PNIPAM solution. Since the excimer fluorescence maximum of the Py$_2$-PNIPAM samples was found to shift with increasing temperatures at temperatures above T_c, the excimer emission was extracted as follows (see Figure S3 in SI). The fluorescence spectrum of the Py$_1$-PNIPAM(25K) sample was used as monomer spectrum since it showed hardly any excimer emission. The spectrum of Py$_1$-PNIPAM(25K) at the desired temperature was normalized to the band at 375 nm of a Py$_2$-PNIPAM fluorescence spectrum. The normalized Py$_1$-PNIPAM(25K) spectrum was subtracted from the Py$_2$-PNIPAM spectrum to yield the excimer fluorescence spectrum. The normalized monomer fluorescence spectra of Py$_1$-PNIPAM(25K) were integrated across their entire wavelength range and the excimer spectra were integrated from 420 to 600 nm to yield I_M and I_E, respectively. The I_M and I_E values were used to calculate the I_E/I_M ratio. The isolated excimer fluorescence spectrum was fitted with a polynomial between 435 and 535 nm to determine the wavelength (λ_{max}) of the fluorescence intensity maximum. Since no shift in excimer fluorescence was observed for the Py$_1$-PNIPAM samples, the I_M and I_E fluorescence intensities were calculated by taking the integral under the fluorescence

signal from 372 to 378 nm and from 500 to 530 nm, respectively.

Analysis of the fluorescence decays was performed with a sum of typically three exponentials as shown in Eq. 1. To ensure the reproducibility of the fluorescence decay analysis, decays were acquired in triplicate.

$$i(t) = \sum_{i=1}^{3} a_i \exp(-t/\tau_i) \qquad (1)$$

The pre-exponential factors and decay times used in Eq. 1 were optimized using the Marquardt−Levenberg algorithm.[39] The quality of the fits was established from the χ^2 values (<1.30) and the random distribution around zero of the residuals and of the autocorrelation function of the residuals.

The number-average ($<\tau>_M$) lifetimes of the pyrene monomer fluorescence decays were calculated using Eq. 2.

$$<\tau>_M = \frac{\sum a_i \tau_i}{\sum a_i} \qquad (2)$$

The parameters a_i and τ_i referred to, respectively, the i^{th} pre-exponential factor and decay time obtained from the multi-exponential fit of the decays with Eq. 1. The number-average lifetime of the excimer $<\tau>_E$ was also obtained by applying Eq. 2 to those decay times with positive pre-exponential factors. Representative pyrene monomer fluorescence decays and the corresponding fluorescence spectra are shown in Figures S4A and S4B, respectively.

RESULTS AND DISCUSSION

Solution properties of Py_n-PNIPAM in water, a brief overview.

Dynamic light scattering measurements performed on aqueous Py_n-PNIPAM solutions kept at 15 °C indicated that, except in the case of the longer semi-telechelic polymers Py_1-PNIPAM(25K) and Py_1-PNIPAM(12K), all polymers self-assembled in water, forming aggregates with hydrodynamic radii (R_h) on the order of 4 to 9 nm, depending on the polymer molar mass and degree of labeling (Table 2). For telechelic polymers, the R_h values increased with increasing molar mass, as observed also in the case of α,ω-dioctadecyl-PNIPAM samples studied previously.[9] By comparing the R_h values of the Py- and C_{18}-telechelic PNIPAMs at temperatures lower than T_c, the Py_2-PNIPAM aggregates were smaller than their $(C_{18})_2$ counterparts, an indication of hydrophobe-induced differences in chain packing within the aggregates.

All Py_n-PNIPAM solutions showed a marked sensitivity to temperature: their turbidity (Figure 1) and light scattered (Figure S5) increased sharply as their temperature exceeded a critical value (T_c), ranging from 16 °C to 31 °C, depending on polymer structure (telechelic-vs-semi-telechelic) and molecular weight. T_c increased with increasing M_n for the Py_1-PNIPAM and Py_2-PNIPAM samples as shown in Figure 1B as a result of the reduction in the content of hydrophobic pyrene associated with an increase in M_n. The trends observed in Figure 1 are consistent with previous studies.[7,9]

The enhanced light scattered by the solutions with temperature (Figure S5) reflected the formation of larger particles. The R_h values of the particles formed at 35 °C were ~ 100 nm (Table 2), a value typical of PNIPAM mesoglobules formed in dilute solution upon dehydration, collapse, and aggregation of PNIPAM chains when heated past their solution cloud point. The R_h values recorded for Py_n-

TABLE 2 Hydrodynamic radii of Lip_n-PNIPAM samples determined by DLS at 15 °C and 35 °C where Lip is either a 1-pyrenenutyl or octadecyl hydrophobe.

Samples	Mw$^{\Delta}$, kDa	$R_h(C_{18})$,[a] nm	$R_h(C_{18})$,[b] nm	R_h(Py),[c] nm (15 °C)	R_h(Py),[d]nm (35 °C)	R_h(Py), nm theoretical
Py_2-PNIPAM	7			5.0±0.2		2.5
	14	10.8	25	5.9±0.4	65	3.6
	25	12.9	28	8.1±0.5	85	4.8
	45	17.5	39	8.9±0.5	100	6.5
Py_1-PNIPAM	7			6.4±0.4		2.5
	12			4.0±1.0		3.3
	25			4.9±0.5		4.8

$^{\Delta}$ M_w provided for $(Py)_2$PNIPAM (analogous masses for (C_{18})2PNIPAM are 12, 22, and 49 kDa, respectively); [a]@ 20 °C and concentration 1 g/L; [b]@ 35 °C and concentration 0.3 g/L; [c]@ 15 °C and concentration 2 g/L; [d]@ 35°C and concentration 0.017, 0.03 and 0.06 g/L for 14, 25 and 45 kDa samples, respectively. Lower Lip_n-PNIPAM concentrations were used at $T > T_c$.

PNIPAM solutions were significantly larger than those of particles obtained with $(C_{18})_2$-PNIPAM solutions at 35 °C (Table 2). The smaller R_h values obtained for Py_2-PNIPAM micelles must have been a result of the less hydrophobic 1-pyrenebutyl end groups, since they were more compact than the octadecyl pendants and thus formed smaller rosette micelles. It is thus interesting that the smaller rosette micelles generated by the Py_2-PNIPAM samples formed much larger mesoglobules compared to the $(C_{18})_2$-PNIPAM samples. The weaker aggregation of the pyrene groups of the Py_2-PNIPAM samples, compared to the C_{18} groups of the $(C_{18})_2$-PNIPAM samples, must have resulted in more dangling pyrene pendants in the corona of the rosette micelles that provided sticky patches to facilitate adhesion of a larger number of rosette micelles at T_c, thus generating larger Py_2-PNIPAM mesoglobules.

The thermal transitions probed by turbidimetry in Figure 1 and light scattering in Figure S5 were obtained for polymer concentration of 0.5 $g.L^{-1}$ and a heating rate of 0.5 $°C.min^{-1}$ and a good agreement was observed for the T_c values obtained by both methods (see Figure 1B). Unfortunately, the information obtained by turbidimetry was difficult to relate to the fluorescence experiments conducted with a much lower polymer concentration and heating rate. As shown in Figures S6A and B, both polymer concentration and heating rate affect T_c substantially, a lower polymer concentration and heating rate resulting in a higher and lower T_c value, respectively. Consequently the turbidity experiments were unable to predict what the T_c value would be for the much more dilute Py_n-PNIPAM solutions used in the fluorescence experiments (see concentrations in Table 1) using a much slower heating rate of about 0.07 $°C.min^{-1}$.

Fluorescence study of aqueous solutions of the telechelic Py_2-PNIPAM samples: The T_c value of the solutions used for the fluorescence experiments was obtained by using the steady-

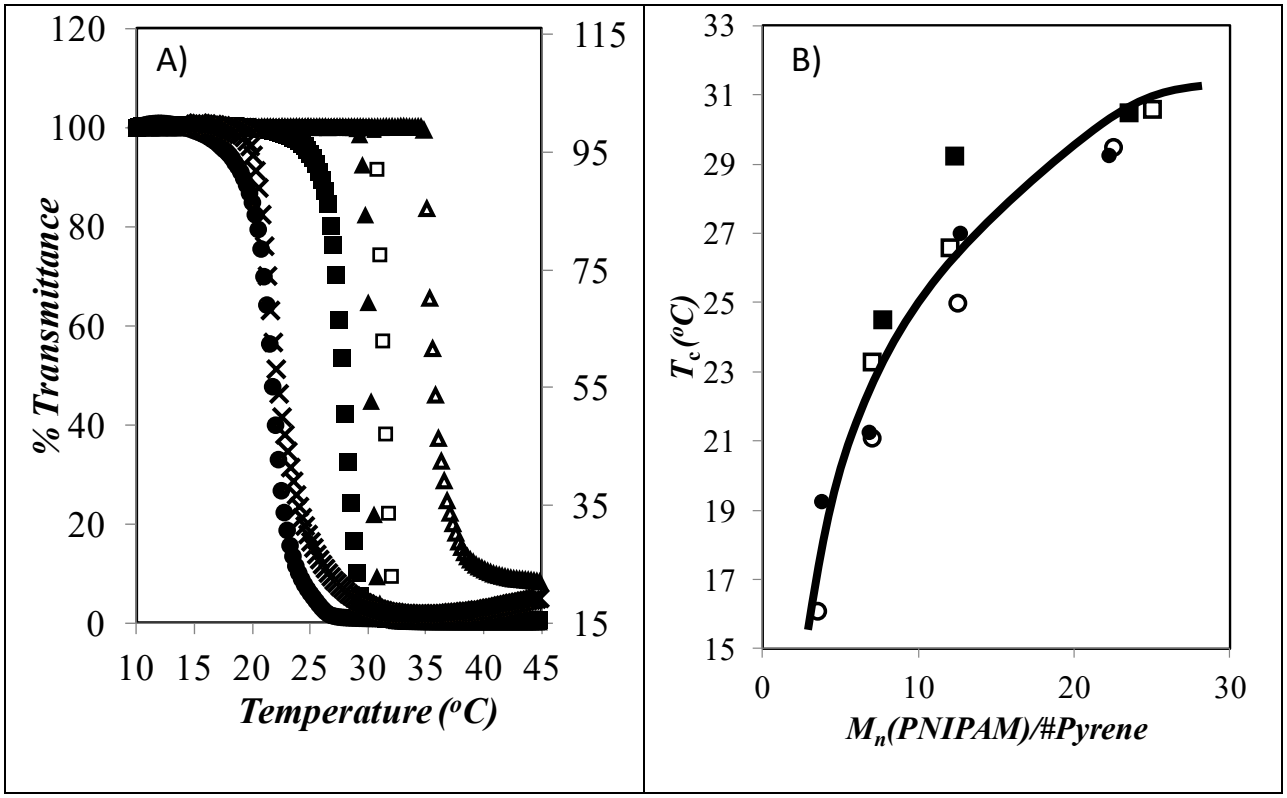

FIGURE 1 Turbidimetry measurements for 0.5 g/L pyrene-labeled PNIPAM samples with a heating rate of 0.5 °C/min. A) (×) Py_2-PNIPAM(7K), (●) Py_2-PNIPAM(14K), (■) Py_2-PNIPAM(25K), (▲) Py_2-PNIPAM(45K), (□) Py_1-PNIPAM(25K), and (Δ) PNIPAM(22K). B) T_c as a function of the ratio of M_n for the Py-PNIPAM samples over their respective number of pyrenes. (●) Py_2-PNIPAM and (■) Py_1-PNIPAM for T_c by turbidimetry, (○) Py_2-PNIPAM and (□) Py_1-PNIPAM for T_c by DLS. Solid line is drawn to guide the eye.

state fluorometer to monitor the light scattered by the more dilute Py_n-PNIPAM aqueous solutions. The right-angle light scattering intensity was measured in the steady-state fluorometer at 500 nm where pyrene does not absorb. The change in light scattering (LS) intensity for aqueous solutions of the Py_2-PNIPAM samples is shown in Figure 2. For all Py_2-PNIPAM samples, the LS intensity increased sharply at a set temperature. The temperature where the LS intensity increased abruptly was taken as the T_c value as done in a previous publication.[37] To this end, lines were drawn through the data points below and above the sharp increase and their intersection point was determined. T_c was found to equal 22, 24, 28, and 28 °C for Py_2-PNIPAM(7K), Py_2-PNIPAM(14K), Py_2-PNIPAM(25K), and Py_2-PNIPAM(45K), respectively. The value of T_c derived from right-angle LS increased with increasing molecular weight, however the increase was not directly proportional to M_n as was observed by turbidimetry and DLS in Figure 1B for a 0.5 $g.L^{-1}$ polymer concentration.

Information on chain end association within the nanoparticles was readily accessible from the fluorescence spectra and decays of the Py_n-PNIPAM solutions that report, respectively, on the extent of pyrene aggregation and the

dynamics of isolated and associated pyrene labels.[40,41] In order to facilitate comparison between the spectra of the various samples, all solutions had the same pyrene concentration of 2.4 µM. The polymer concentration of the solutions ranged from 9.5 mg.L^{-1} for Py_2-PNIPAM(7K) to 56 mg.L^{-1} for Py_2-PNIPAM(45K) as the longer chains required a larger massic concentration to achieve a same pyrene concentration as the shorter chains. The spectra obtained for the Py_2-PNIPAM(14K) solution, normalized to the intensity of the I_1 peak of the pyrene monomer at 375 nm, are presented in Figure 3. The intensity of the excimer increased as the temperature increased until T_c was reached, at which point the excimer intensity decreased and its wavelength maximum underwent a blue shift.

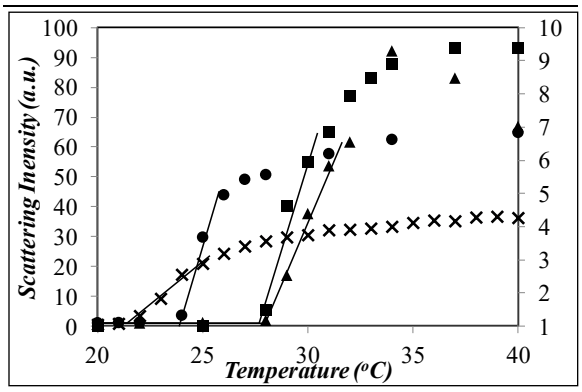

FIGURE 2 Normalized light scattering intensity of Py_2-PNIPAM samples as a function of temperature, Abs(342nm) = 0.1. (×, right axis, 9.5 mg.L^{-1}) Py_2-PNIPAM(7K), (●, left axis, 17 mg.L^{-1}) Py_2-PNIPAM(14K), (■, right axis, 32 mg.L^{-1}) Py_2-PNIPAM(25K), and (▲, left axis, 56 mg.L^{-1}) Py_2-PNIPAM(45K).

Changes in the relative excimer intensity reflect different interactions between the hydrophobic

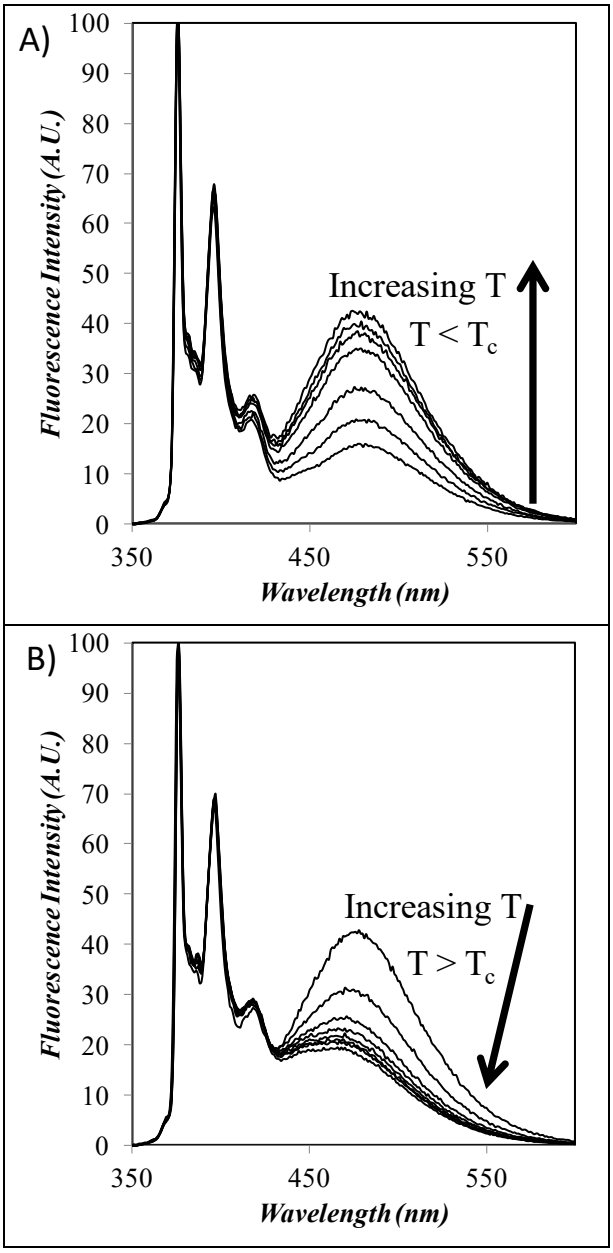

FIGURE 3 Steady-state fluorescence spectra for Py_2-PNIPAM(14K) at different temperatures. A) *T* increases from 15 to 23 °C. B) T increases from 24 to 40 °C.

pyrene groups. Since steady-state fluorescence of pyrene reports directly on the behavior of the hydrophobic groups within a Py_2-PNIPAM polymer, the relationship between temperature and excimer fluorescence intensity was further investigated by the determination of the ratio of the fluorescence intensity of the excimer

over that of the monomer, namely the I_E/I_M ratio. The position of the excimer fluorescence maximum (λ_{max}) was also determined. Both I_E/I_M and λ_{max} are shown in Figure 4 for all the Py_2-PNIPAM constructs.

All Py_2-PNIPAM samples showed a maximum value in I_E/I_M at the same temperature where a sharp increase in light scattering intensity was observed in Figure 2. The increase in I_E/I_M at temperatures lower than T_c indicates an increase in the local pyrene concentration $[Py]_{loc}$ due to a contraction of the polymer coil. Although the coil size might decrease while I_E/I_M increases with increasing temperature in Regime I, no significant decrease in light scattering was observed over the same temperature range (see Figure 2), probably because the polymer species did not scatter much below T_c in the first place. Following this increase, I_E/I_M reached a maximum at or near T_c before beginning to decrease with increasing temperature. The origin of the decrease in I_E/I_M above T_c could be inferred from the observation that the excimer emission maximum in Figure 3B shifted to lower wavelengths. The plot of the wavelength at the maximum fluorescence intensity of the excimer (λ_{max}) as a function of temperature in Figure 4B confirmed that λ_{max} began to decrease at T_c, a temperature regime corresponding to Region II. The blue shift in the excimer emission wavelength indicates an increase in the relative amount of aggregated pyrene[42,43] taking place after the polymer underwent its cloud point transition and entered Regime II.

The decrease in I_E/I_M above T_c was certainly caused by a decrease in the mobility of pyrene, since this would decrease the amount of excimer being formed by diffusion, favor excimer formation by direct excitation of a pyrene aggregate, and result in the shift in λ_{max} observed in Figure 4B. The dehydrating PNIPAM coils collapsed above T_c to form stiffer domains composed of dehydrated PNIPAM chains that hindered diffusive encounters between the pyrene labels, thus leaving the aggregated pyrenes with their blue-shifted emission as the main excimer species in solution. The decrease in I_E/I_M and shift in λ_{max} observed in Figure 4 at temperatures larger than T_c continued up to 31 °C for all Py_2-PNIPAM samples above which no further change was found suggesting that 31 °C marked the end of Regime II represented by T_m. The continued decrease in λ_{max} after T_m observed in Figure 4B for Py_2-PNIPAM(45K) is due to the very low amount of excimer obtained with this sample which made it more challenging to estimate λ_{max} (compare I_E/I_M values in Figure 4A for the Py_2-PNIPAM(45K) sample for $T > 31$ °C).

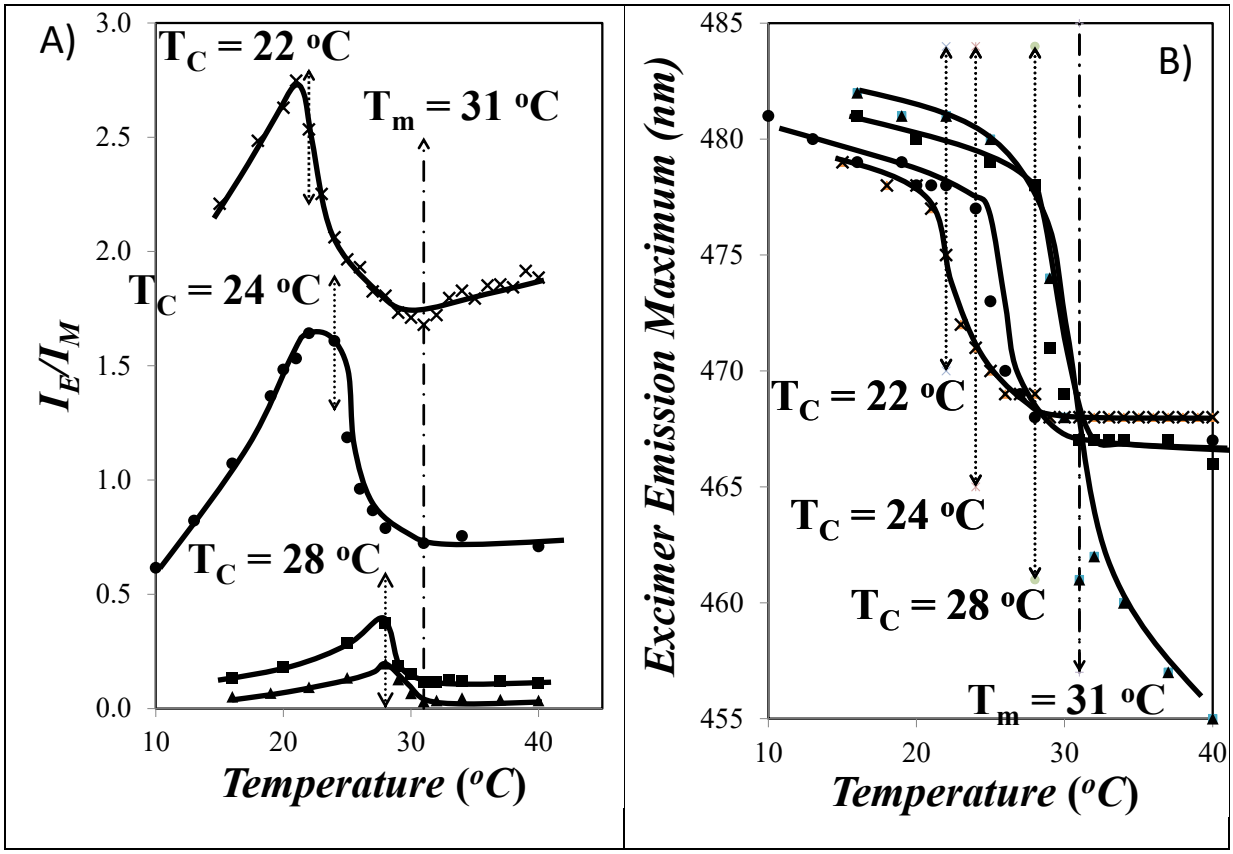

FIGURE 4 A) I_E/I_M ratio for the Py_2-PNIPAM samples in water as a function of temperature and B) wavelength at the excimer intensity maximum, Abs(342 nm) = 0.1. (×) Py_2-PNIPAM(7K), (●) Py_2-PNIPAM(14K), (■) Py_2-PNIPAM(25K), and (▲) Py_2-PNIPAM(45K)

In order to further investigate the origin of the decrease in I_E/I_M at T_c, time-resolved fluorescence decays of the pyrene monomer and excimer of Py_2-PNIPAM aqueous solutions were acquired. The decays were analyzed by performing a tri-exponential fit with Eq. 1, and the number-average lifetime, $\langle\tau\rangle_M$, of the pyrene monomer decay was plotted as a function of temperature in Figure 5. The determination of T_c from the trends obtained with $\langle\tau\rangle_M$ was carried out according to the same protocol which was used for LS. A detailed error analysis of the value of T_c was prevented by the small number of data points in the linear region above T_c, leading to an unrealistic propagated error of up to 10 °C. The resolution of the temperature controller was 1 °C. Therefore, the error in the value of T_c based on trends obtained with $\langle\tau\rangle_M$ in Figure 5 should not be significantly larger than 1 °C.

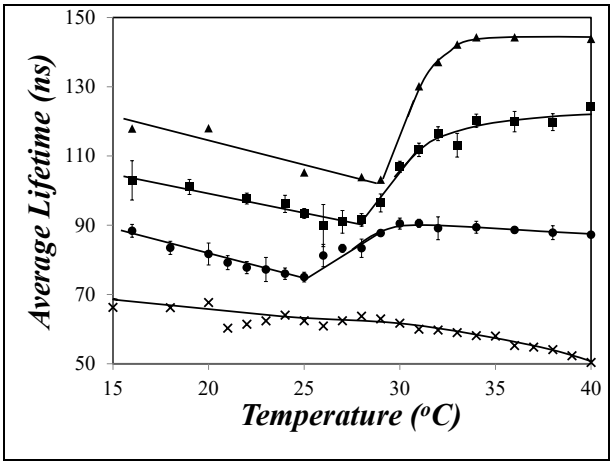

FIGURE 5 Number-average lifetime of the pyrene monomer decays for the pyrene labeled PNIPAM samples in water as a function of temperature. (×) Py_2-PNIPAM(7K), (●) Py_2-PNIPAM(14K), (■) Py_2-PNIPAM(25K), and (▲) Py_2-PNIPAM(45K).

At temperatures lower than T_c, $<\tau>_M$ was found to decrease with increasing temperature for the Py_2-PNIPAM(14K), Py_2-PNIPAM(25K), and Py_2-PNIPAM(45K) samples. Above their respective T_c of 25 °C, 28 °C, and 29 °C, $<\tau>_M$ increased with increasing temperature up to a temperature of ~32-33 °C indicating the end of Regime II marked by T_m. The T_c and T_m values determined using $<\tau>_M$ were slightly higher than those obtained with I_E/I_M or light scattering, implying that parameters retrieved from the pyrene monomer fluorescence decays may be less sensitive to the changes occurring in solution than parameters derived from steady-state fluorescence spectra. The Py_2-PNIPAM(7K) sample showed little change in $<\tau>_M$ at T_c and T_m, likely due to the small amount of monomer emission present in this sample since the pyrenes are strongly aggregated to start with and the short PNIPAM chain does not afford much protection against quenching by oxygen dissolved in the aqueous phase. The decrease in $<\tau>_M$ observed for the higher molecular weight Py_2-PNIPAM samples (M_n = 12, 25, and 45K) as the temperature increased toward T_c might be reasonably explained by an increase in the amount of excimer being formed by diffusion as the overall dimension of the polymer chain decreases with increasing temperature thus bringing the pyrene labels close from each other. This is supported by the increase in I_E/I_M ratio observed in Figure 4 indicating increased excimer formation.

Above T_c, the monomer lifetime increased significantly due to the collapse of the dehydrated PNIPAM that induced either a decrease in the quenching efficiency of oxygen, a decrease in the rate of excimer formation by diffusion due to decreased local mobility, or a combination of both. For the longer Py_2-PNIPAM(45K) sample whose pyrene monomer decayed quasi monoexponentially and did not form much excimer, the increase in $<\tau>_M$ suggested a reduction in oxygen quenching efficiency since very little excimer was generated by this sample, but the longer PNIPAM chain afforded good protection against quenching by oxygen. All these results agreed with the steady-state fluorescence data, showing a maximum level of excimer formation around T_c and a continuous decrease in excimer formation by diffusion due to stiffening of the dehydrating PNIPAM throughout Regime II up to a temperature T_m of ~31-33 °C depending on sample and type of experiment. Accordingly, $<\tau>_M$ reported on the behaviour of the hydrophobes rather than the behaviour of the entire polymer chain as the solution temperature increased from below T_c to above T_m, thus covering the entire process depicted in Scheme 1.

Having accounted for the trends obtained from the analysis of the monomer decays, the results obtained from the analysis of the excimer decays were interpreted. As for the monomer decays, multi-exponential fits of the excimer decays were also performed, and the average lifetime of the excimer $<\tau>_E$ and the ratio a_{E-}/a_{E+} were plotted as a function of solution temperature in Figure 6. The ratio a_{E-}/a_{E+}, equal to the sum of the negative pre-exponential factors over the sum of the positive pre-exponential factors retrieved from the fit of the excimer decay with Eq. 1, is a measure of the amount of excimer formed by diffusion. A value of 0 for a_{E-}/a_{E+} indicates full aggregation while a value of −1 indicates purely diffusion-controlled excimer formation.

At temperatures below T_c, $<\tau>_E$ equaled 65 ± 2 ns. The $<\tau>_E$ values for Py_2-PNIPAM in Figure 6A showed a significant increase at the expected T_c of the samples, based on the temperatures which were seen to affect the monomer decays in Figure 5. As with the monomer decays, $<\tau>_E$ increased at temperatures greater than T_c due

to decreased oxygen quenching and slower diffusion for excimer formation. The increase in $<\tau>_E$ continued up to T_m = 32 °C for all Py_2-PNIPAM samples except Py_2-PNIPAM(7K). As already mentioned, strong pyrene aggregation and the short PNIPAM chain of Py_2-PNIPAM(7K), which did not offer much protection to the pyrene labels against oxygen dissolved in water, were responsible for the weaker response experienced by the parameters retrieved from the analysis of the fluorescence data obtained with this sample. Otherwise the general trend for a_{E-}/a_{E+} agreed with the trends obtained with the other parameters earlier. The ratio a_{E-}/a_{E+} took a negative value just before T_c that was equal to −0.10, −0.32, −0.35, and −0.36 for, respectively, the 7, 14, 25, and 45K Py_2-PNIPAM samples. The more negative ratios obtained for longer constructs indicate that the longer chains result in a larger molar fraction of pyrene labels forming excimer by diffusion, albeit at a much slower rate. The a_{E-}/a_{E+} ratio became less negative at T_c due to an increase in the molar fraction of aggregated pyrenes and a decrease in excimer formation by diffusion due to the reduced mobility experienced by the PNIPAM backbone above T_c. These changes in the behaviour of a_{E-}/a_{E+} started at T_c and ended

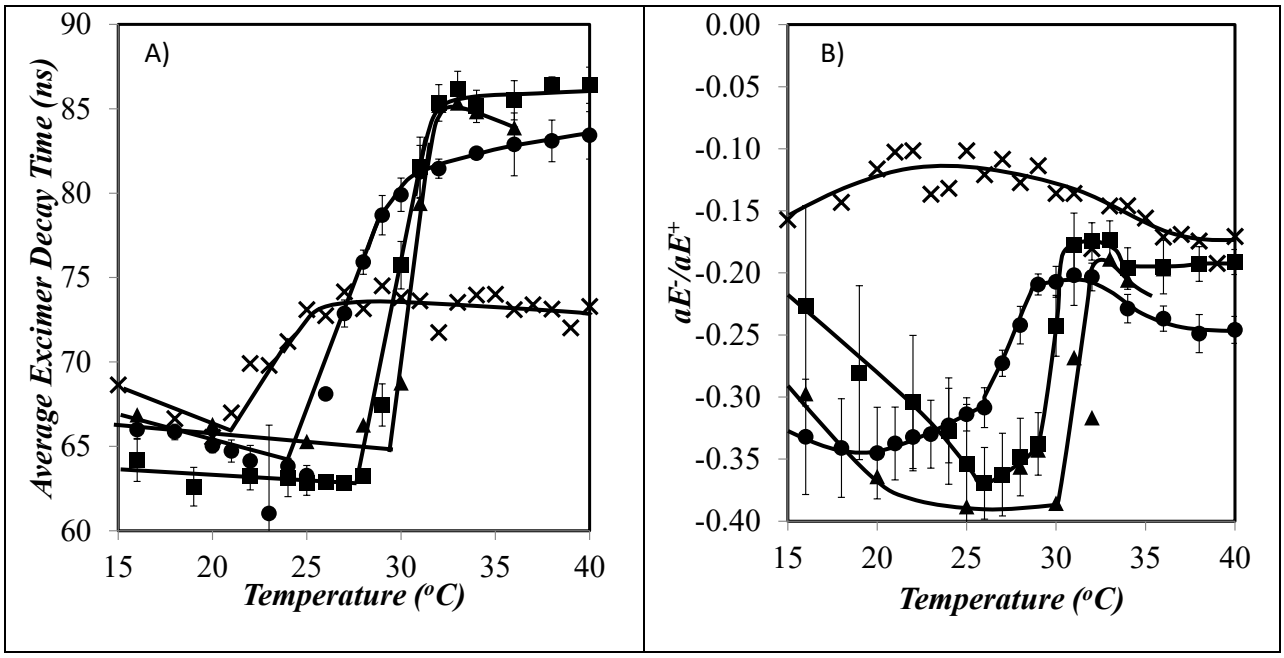

FIGURE 6 A) $<\tau_N>_E$ obtained with decay times having positive pre-exponential factors and B) a_{E-}/a_{E+} ratio as a function of solution temperature. (×) Py_2-PNIPAM(7K), (●) Py_2-PNIPAM(14K), (■) Py_2-PNIPAM(25K), and (▲) Py_2-PNIPAM(45K)

at a temperature of ~32 °C which was attributed to T_m marking the end of Regime II. The large error bars observed for Py_2-PNIPAM(25K) below T_c reflected large variations in a_{E-}/a_{E+} for decays obtained in this temperature range. The lack of a clear transition in a_{E-}/a_{E+} for the Py_2-PNIPAM(7K) sample was likely due to the more positive value of a_{E-}/a_{E+} below T_c (= 22 °C), which is approximately equal to the value of a_{E-}/a_{E+} above T_c, a consequence of the strong level of pyrene aggregation experienced by this sample.

At this stage, the light scattering intensity, the I_E/I_M ratios, the wavelength at the excimer fluorescence intensity maximum (λ_{max}), the average monomer $<\tau>_M$ and excimer $<\tau>_E$ decay

times, and the ratio a_{E-}/a_{E+} were found to all undergo significant changes around T_c and T_m for each sample studied. The T_c values retrieved from the trend obtained with each parameter have been reported in Table 3. As the T_c values showed a fairly narrow distribution, they were best reported as an aggregate value, all of which are shown in Table 3. T_m did not change much with M_n and was found to equal 32 ± 1 °C.

The cloud point transition temperature of each solution was taken as the average of the T_c values measured by the different techniques and listed in Table 3. As shown in Table 3, a maximum spread of approximately 1.3 °C is obtained for all three Py_2-PNIPAM samples, likely due to the fact that certain techniques probe the transition at either the high or low end of the temperature distribution. Light scattering, I_E/I_M, and λ_{max} gave the lowest transition temperatures, while the a_{E-}/a_{E+} ratio retrieved from the fluorescence decay analysis gave the highest transition temperatures, implying that lifetime-derived parameters may not be as sensitive to the cloud point transition. The molecular weight dependence of T_c can also be observed using the aggregate T_c values, where T_c increases with increasing molecular weight up to 25K with the Py_2-PNIPAM(25K) and Py_2-PNIPAM(45K) samples yielding similar T_c values.

TABLE 3 T_c values obtained from the study of aqueous solutions of the Py_2-PNIPAM samples with different techniques.

Sample	T_c (°C) as determined by:						
	L.S.	I_E/I_M	λ_{max}	$\langle\tau_N\rangle_M$	$\langle\tau_N\rangle_E$	a_{E-}/a_{E+}	Average
Py_2-PNIPAM(7K)	22	22	21	a)	21	a)	21.5 ± 0.5
Py_2-PNIPAM(14K)	24	24	24	25	24	27	25.0 ± 1.2
Py_2-PNIPAM(25K)	28	28	28	28	28	30	28.6 ± 1.0
Py_2-PNIPAM(45K)	28	28	28	29	29	31	29.1 ± 1.3

[a)] No transition was detected with this parameter.

Fluorescence study of aqueous solutions of the semi-telechelic Py_1-PNIPAM samples: The study with the Py_2-PNIPAm samples suggested that the hydrophobic pyrene labels responded to the changes experienced by the PNIPAM backbone as a function of temperature. To confirm that this was indeed the case, the experiments were repeated with the semitelechelic Py_1-PNIPAM samples. The light scattering intensity, the I_E/I_M ratio, and the decay times $\langle\tau\rangle_M$ were obtained from the analysis of the steady-state fluorescence spectra and time-resolved fluorescence decays of aqueous solutions of Py_1-PNIPAM(7K), Py_1-

PNIPAM(12K), and Py_1-PNIPAM(25K). The trends obtained by plotting these parameters as a function of temperature are shown in Figure 7.

The light scattering intensity, presented in Figure 7A, shows a sharp increase at 30 °C for all three samples. Based on the trends obtained by light scattering, the transition at 30 °C was assigned to T_c in good agreement with the turbidimetry results presented in Figure S6A that showed that T_c for the semitelechelic samples seemed to cluster around 30 °C as the polymer concentration decreased. The I_E/I_M ratio in Figure 7B underwent significant changes for the Py_1-PNIPAM(7K) and Py_1-PNIPAM(12K) samples as the temperature increased past T_c, while I_E/I_M remained small and relatively constant for Py_1-PNIPAM(25K). The $<\tau>_M$ behavior of the Py_1-PNIPAM(12K) and Py_1-PNIPAM(25K) samples shown in Figure 7C closely resembled that of the Py_2-PNIPAM samples, increasing at T_c and plateauing above T_m while the Py_1-PNIPAM(7K) showed no clear transition at T_c.

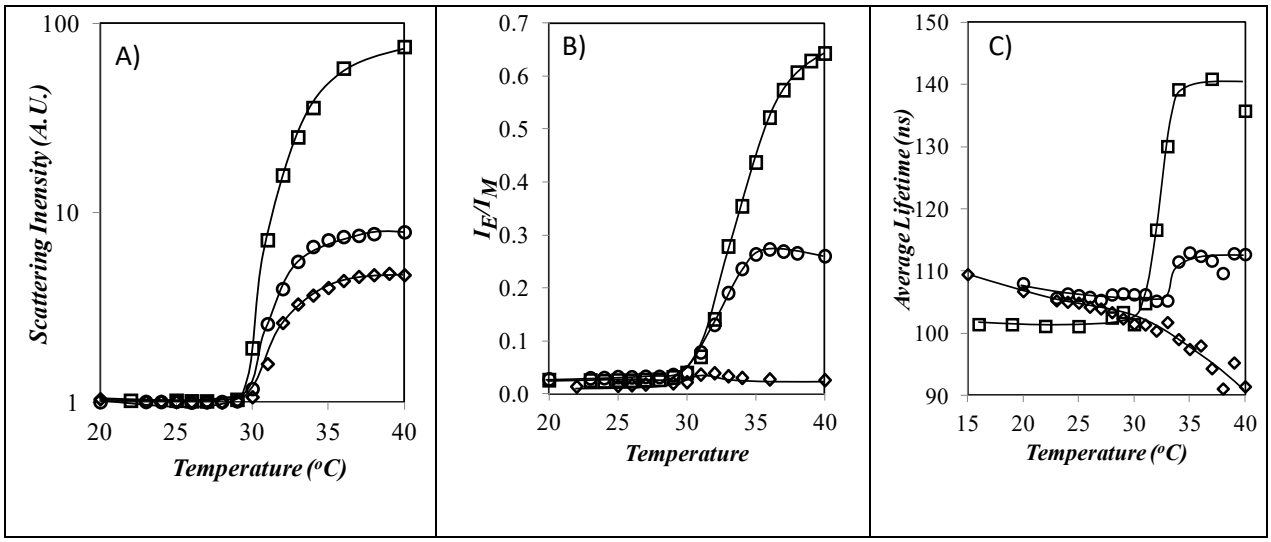

FIGURE 7 Light scattering and fluorescence results for aqueous solutions of the Py_2-PNIPAM samples. (◊) Py_1-PNIPAM(7K), (○) Py_1-PNIPAM(12K), and (□) Py_1-PNIPAM(25K). A) Light scattering intensity.; B) I_E/I_M; C) $<\tau>_M$.

The trends observed with the Py_1-PNIPAM samples exhibited some features that were similar to those obtained with the Py_2-PNIPAM samples. In particular, the light scattering intensity, I_E/I_M, and $<\tau>_M$ showed a pronounced change at T_c. There were however significant differences between the two families of Py_n-PNIPAM samples. The Py_1-PNIPAM samples did not show any M_n-dependence with regard to T_c as determined by light scattering, I_E/I_M, or $<\tau>_M$. $<\tau>_M$ remained constant with temperature in Regime I, and I_E/I_M did not pass through a maximum at T_c but instead, began to increase with increasing temperature once T_c was reached for the Py_1-PNIPAM(12K) and Py_1-PNIPAM(25K) samples.

The differences in behavior for $<\tau>_M$ and I_E/I_M between the Py_1-PNIPAM samples and their corresponding Py_2-PNIPAM samples were best explained by the fact that Py_1-PNIPAM formed significantly less excimer than Py_2-PNIPAM, a consequence of the inability of the semi-telechelic samples to form micelles below T_c as

confirmed by the R_H values of the 12 and 25K Py_1-PNIPAM constructs whose R_h measured by DLS matched the predicted values for isolated coils in Table 2. The difference between measured and predicted R_h values for Py_1-PNIPAM(7K) in Table 2 suggests that this sample forms polymeric aggregates at the concentration of 2 $g.L^{-1}$ used in the DLS experiments. However the absence of excimer fluorescence in Figure 7B indicates that no Py_1-PNIPAM(7K) aggregates form at the concentration of 17 $mg.L^{-1}$ used in the fluorescence experiments, certainly a consequence of the much lower polymer concentration. As the temperature increased in Regime I, $<\tau>_M$ and I_E/I_M for Py_1-PNIPAM remained constant because each chain contained only one pyrene. Thus a decrease in the radius of gyration of the chains did not change the local pyrene concentration and thus had no effect on pyrene excimer formation for these singly labeled chains. When mesoglobules formed in Regime II, the significant reduction in the mobility of pyrene did not result in a decrease in I_E/I_M as was observed for the Py_2-PNIPAM polymers in Figure 4A since very little diffusional excimer was present before the transition which could be affected by this change. Instead, the aggregation of chains into larger particles actually increased the local pyrene concentration and allowed more excimer to form.

Agreement between fluorescence data and Scheme 1: The light scattering and fluorescence trends observed thus far are best explained using the model developed by Winnik et al. for *lip*$_2$-PNIPAM in aqueous solution (see Scheme 1).[9,15,18] In Regime I, the Py_2-PNIPAM chains in solution are primarily found in polymeric micelles or single chains. These solutions exhibit low light scattering intensity due to the small size of the micelles and chains. The hydrophobic pyrenes are relatively exposed to the solution resulting in shorter monomer and excimer lifetimes due to greater exposure to oxygen dissolved in the aqueous phase. As the temperature increases in Regime I, the size of the micelles decreases which increases the local pyrene concentration, resulting in an increase in I_E/I_M and a slight decrease in $<\tau>_M$.

At T_c, the solutions enter Regime II which results in the formation of mesoglobules. The resulting increase in particle size, observed by DLS, causes an increase in both the turbidity and light scattering signals. The larger particles are better able to protect pyrene from quenching by oxygen in the solution, causing an increase in $<\tau>_M$ and $<\tau>_E$. The more hindered diffusion within the dehydrated mesoglobules reduces the mobility of the pyrene labels, reducing their ability to form excimer by diffusion; this causes a blue-shift in the wavelength of maximum excimer emission, a decrease in I_E/I_M, and an increase in the a_{E-}/a_{E+} ratio. The changes that occur at T_c for these parameters continue into Regime II, until they plateau at or before T_m. Above T_m in Regime III all parameters remain constant. These observed trends for light scattering and fluorescence parameters are consistent with the predictions made by the model proposed by Winnik et al. for aqueous *lip*$_2$-PNIPAM.

CONCLUSIONS

The use of fluorescence to probe the behaviour of aqueous solutions of pyrene end-labeled PNIPAMs has demonstrated that the behaviour of the hydrophobic pyrene labels is intimately linked to that of the polymeric constructs as similar transitions were observed by LS which probes the entire polymer and fluorescence

that only probes the end groups. Turbidimetry and light scattering have shown that the value of T_c depends on the hydrophobe content of the telechelic polymers, which is consistent with earlier work.[7] Analysis of the steady-state fluorescence spectra and the time-resolved fluorescence decays yielded a set of parameters indicating that the pyrene labels responded to changes in polymer conformations induced by changes in solution temperature as the solution temperature increased past a T_c value that depended on PNIPAM chain length and a T_m value that seemed little affected by PNIPAM chain length. Most importantly, the behavior of the pyrenyl groups probed by fluorescence agreed very well with expectations based on the model presented in Scheme 1.

The Py_1-PNIPAM samples showed significant behavioral changes at T_c. Even though the change in behaviour was different from that observed with the Py_2-PNIPAM samples, these differences could be traced back to the differences in the ability of telechelic and semi-telechelic PNIPAM to form pyrene excimer. All light scattering and fluorescence results were largely consistent with the model developed by Winnik et al. for *lip*$_2$-PNIPAM in aqueous solution.[9,15-18] Specifically, the decrease in micellar size in Regime I and the formation of mesoglobules in Regime II have been confirmed via light scattering, steady-state, and time-resolved fluorescence measurements.

Finally, the fact that the dehydration of the Py_n-PNIPAM samples could be observed by light scattering that probes the entire polymer coil and pyrene fluorescence that probes the hydrophobic end groups only is quite remarkable since the dehydration of the Py_n-PNIPAM samples is believed to start with the PNIPAM segments located close to the hydrophobic end groups. This observation demonstrates that PNIPAM dehydration, which occurs first at the chain ends, affects the behavior of the entire chains, at least for the Py_n-PNIPAM constructs that were investigated in this study.

ACKNOWLEDGEMENTS

The authors thank NSERC for financial support of this research.

SUPPORTING INFORMATION

Analysis of the fluorescence spectra, comparison between fluorescence spectra and decays, procedure to determine T_c by turbidimetry, tables with FWHM and T_c obtained by two different methods for the turbidimetry measurements.

REFERENCES AND NOTES

1. M. Heskins, J. E. Guillet, *J. Macromol. Sci.: A - Chem.* **1968**, *2*, 1441-1445.
2. M. Duan, S. Fang, H. Guo, L. Zhang, *J. Macromol. Sci. B Phys.* **2009**, *48*, 834-843.
3. H. Yang, R. Cheng, Z. A. Wang, *Polymer* **2003**, *44*, 7175-7180.
4. Z. Fang, T. Zhen, *Sci. in China Ser. B* **1998**, *42*, 290-297.
5. N. Ishii, J. Mamiya, T. Ikeda, F. M. Winnik, *Chem. Commun.* **2011**, *47*, 1267-1269.
6. Y. Mylonas, G. Bokias, I. Iliopoulos, G. Staikos, *Eur. Polym. J.* **2006**, *42*, 849-857.
7. X. Qiu, T. Koga, F. Tanaka, F. M. Winnik, *Sci. China Chem.* **2013**, *56*, 56-64.
8. R. Pamies, K. Zhu, A. Kjoniksen, B. Nystrom, *Polym. Bull.* **2009**, *62*, 487-502.
9. P. Kujawa, F. Tanaka, F. M. Winnik, *Macromolecules* **2006**, *39*, 3048-3055.
10. R. Nojima, T. Sato, X. Qiu, F. M. Winnik, *Macromolecules* **2008**, *41*, 292-294.

11. J. Yip, J. Duhamel, X. P. Qiu, F. M. Winnik, *Can. J. Chem.* **2011**, *89*, 163-172.
12. J. Yip, J. Duhamel, X. P. Qiu, F. M. Winnik, *Macromolecules* **2011**, *44*, 5363-5372.
13. C. K. Chee, S. Rimmer, I. Soutar, L. Swanson, *Polymer* **1997**, *38*, (2), 483-486.
14. I. Iliopoulos, J. L. Halary, R. Audebert, *J. Polym. Sci. A* **1988**, *26*, 275-284.
15. T. Koga, F. Tanaka, R. Motokawa, S. Koizumi, F. M. Winnik, *Macromolecules* **2008**, *41*, 9413-9422.
16. F. Tanaka, T. Koga, H. Kojima, F. M. Winnik, *Chin. J. Polym. Sci.* **2011**, *29*, 13-21.
17. T. Koga, F. Tanaka, R. Motokawa, S. Koizumi, F. M. Winnik, *Macromol. Symp.* **2010**, *291-292*, 177-185.
18. F. Tanaka, T. Koga, I. Kaneda, F. M. Winnik, *J. Phys.: Condens. Matter* **2011**, *23*, 284105-284112.
19. H. G. Schild, *Prog. Polym. Sci.* **1992**, *17*, (2), 163-249.
20. F. Afroze, E. Nies, H. Berghmans, *J. Mol. Structure* **2000**, *554*, (1), 55-68.
21. R. G. de Azevedo, L. P. N. Rebelo, A. M. Ramos, J. Szydlowski, H. C. de Sousa, J. Klein, *Fluid Phase Eq.* **2001**, *185*, 189-198.
22. L. P. N. Rebelo, Z. P. Visak, H. C. de Sousa, J. Szydlowski, R. G. de Azevedo, A. M. Ramos, V. Najdanovic-Cisak, M. N. da Ponte, J. Klein, *Macromolecules* **2002**, *35*, 1887-1895.
23. A. Milewska, J. Szydlowski, L. P. N. Rebelo, *J. Polym. Sci. Polym. Phys. Ed.* **2003**, *41*, 1219-1233.
24. Y. Okada, F. Tanaka, *Macromolecules* **2005**, *38*, 4465-4471.
25. P. Kujawa, V. Aseyev, H. Tenhu, F. M. Winnik, *Macromolecules* **2006**, *39*, 7686-7693.
26. P. Kujawa, V. Aseyev, H. Tenhu, F. M. Winnik, *Macromolecules* **2006**, *39*, 7686-7693.
27. S. Fujishige, K. Kubota, I. Ando, *J. Phys. Chem.* **1989**, *93*, 3311-3313.
28. F. Tanaka, T. Koga, F. M. Winnik, *Progr. Colloid Polym. Sci.* **2009**, *136*, 1-8.
29. J. Škvarla, R. K. Raya, M. Uchman, J. Zednik, K. Procházka, V. M. Garamus, A. Meristoudi, S. Pispas, M. Štěpánek, *ASAP Colloid Polym. Sci.* **2017**.
30. H. Rinsdorf, J. Venzmer, F. M. Winnik, *Angew. Chem. Int. Ed. Engl.* **1991**, *30*, 315-318.
31. X. Wang, L. Li, *Polymer* **2016**, *88*, 123-132.
32. C.-T. Lai, R.-H. Chien, S.-W. Kuo, J.-L. Hong *Macromolecules* **2011**, *44*, 6546-6556.
33. Hydrophilic Polymers: Performance with Environmental Acceptability; Glass, J. E.; Ed.; American Chemical Society: Washington, DC, 1996, Vol. 248.
34. Associative Polymers in Aqueous Solution: Glass, J. E., Ed.; American Chemical Society: Washington, DC, 2000, Vol. 765.
35. Z. Li, S. O. Kyerematen, K. Fuchise, R. Kakuchi, R. Sakai, T. Kakuchi, J. Kressler, *Macromol. Chem. Phys.* **2009**, *210*, 2138-2147.
36. L. M. Johnson, Z. Li, A. J. LaBelle, F. S. Bates, T. P. Lodge, M. A. Hillmyer, *Macromolecules* **2017**, *50*, 1102-1112.
37. P. Kujawa, F. Segui, S. Shaban, C. Diab, Y. Okada, F. Tanaka, F. M. Winnik, *Macromolecules* **2006**, *39*, 341-348.
38. F. M. Winnik, *Chem. Rev.* **1993**, *93*, 587-614.
39. W. H. Press, B. P. Flannery, S. A. Teukolsky, W. T. Vetterling, *Numerical Recipes. The Art of Scientific Computing (Fortran Version)*; Cambridge University Press: Cambridge, 1992.

40. J. Duhamel, *Langmuir* **2012**, *28*, 6527-6538.
41. J. Duhamel, *Langmuir* **2014**, *30*, 2307-2324.
42. O. A. Khakhel, *J. Appl. Spec.* **2001**, *68*, 280-286.
43. A. K. Dutta, T. N. A. Misra, *Langmuir* **1996**, *12*, 459-465.

Table of Content